J. Fluid Mech. (2004), *vol.* 502, *pp.* 1–16.
DOI: 10.1017/S0022112003007201 Printed in the United Kingdom

Revisiting the linear theory of sand dune formation

By M. COLOMBINI

Dipartimento di Ingegneria Ambientale, Università degli Studi di Genova,
Via Montallegro 1, 16145 Genova, Italy

(Received 6 August 2001 and in revised form 3 July 2003)

A linear stability theory for dune and antidune formation is presented that implements a rotational two-dimensional flow model. As in previous linear theories, the phase-lag between sediment transport and bed elevation remains the main mechanism driving instability. However, it is shown that this phase-lag varies significantly in a neighbourhood of the bed. Moreover, since the layer in which sediments are moving has a finite (though small) thickness, it is assumed that the perturbations of the fluid stress driving bedload transport should be evaluated at the top of the layer itself. It is shown that such an apparently minor modification of the classical approach alters remarkably the balance between stabilizing and destabilizing effects that drives the instability process. This also allows a clarification of the debated role of bedslope on the formation of dunes and antidunes. Following the above ideas, antidunes are shown to form in the absence of suspended sediment load and without any effect associated with sediment inertia. The present analysis ultimately allows a successful unification of the theories of dune and antidune formation.

1. Introduction

Forty years ago, Kennedy (1963) published his seminal paper on the mechanism of formation of dunes and antidunes in erodible channels. The real breakthrough of this work, further assessed in Kennedy (1969), was undoubtedly to show that bedforms can be interpreted as periodic perturbations of the shape of the river bed that interact with the flow, creating a dynamic system that can experience temporal growth or decay according to an instability mechanism.

Coupling a suitable flow model to the continuity equation for the sediment phase, several researchers were able to apply this concept to the study of bedforms of different scales and spatial patterns, making use of techniques developed in the field of hydrodynamic stability. The impact on the newborn field of morphodynamics was striking. Dunes, antidunes and fluvial ripples were investigated by means of linear stability analyses by, among others, Engelund (1970), Hayashi (1970), Fredsøe (1974), Richards (1980), Engelund & Fredsøe (1982) and Sumer & Bakioglu (1984), soon followed by bars (Callander 1969), meanders (Ikeda, Parker & Sawai 1981; Blondeaux & Seminara 1985), and also, more recently, by ridges (Tsujimoto 1989; Colombini 1993) as well as streaks (Colombini & Parker 1995) and sorting waves (Seminara, Colombini & Parker 1996).

All these analyses claim to be able to predict the existence of unstable regions in the parameter space, together with the wavelength of the most unstable disturbance, assumed to be the one that will eventually prevail during the amplification process. In general, the agreement of theoretical predictions with experimental observations is

fairly good, thus showing that the basic mechanism of bedform formation is indeed an instability mechanism.

A simple glance at the linearized form of the Exner's equation (see § 4) reveals that if the local sediment transport rate is exactly in phase with bed elevation, no amplification of bed perturbation is obtained. The phase-lag between sediment transport and bed topography is therefore the actual mechanism of instability. Several effects contribute to this lag, bed evolution being ultimately due to a subtle balance between stabilizing and destabilizing effects, among the latter bed friction being the most effective.

In the formulation of the linear stability analysis of bedforms an essential role is played by the flow model, which is responsible for the evaluation of the bed shear stress that, in turn, drives the bed evolution. On the basis of the flow model used, existing linear stability theories for dunes and antidunes can be grouped into three main categories: potential flow (Kennedy 1963; Parker 1975; Coleman & Fenton 2000), shallow-water (Gradowczyk 1970) and rotational solutions (Engelund 1970; Smith 1970; Fredsøe 1974; Richards 1980). Depending on the flow model used, the bed shear stress can or cannot lag the bed profile. In this regard, the choice of the flow model becomes crucial. Potential flow analyses (with the notable exception of Coleman & Fenton (2000), whose contribution will be briefly discussed in the final section) produce no lag, while shallow-water theories invariably predict stability of a uniform steady flow. Rotational flow models provide the most accurate description of the linearized bed shear stress distribution.

On the sediment transport side, sediment suspension (Fredsøe 1974) or particle inertia (Parker 1975) are known to introduce some delay in the response of sediment transport to the driving action of the flow, ultimately resulting in a lag between the sediment discharge and the flow itself. Finally, when only bedload transport is considered, gravity favours the downhill motion of the grains and conversely opposes the uphill motion, again producing a (stabilizing) lag.

Once all the necessary ingredients are inserted in a linear stability analysis of dune and antidune formation, a clear picture of the mechanism that drives the instability process should emerge. In this regard, none of the existing theories is entirely satisfactory, as it will be shown in the following.

In the present contribution, a rotational and linear stability model of plane flow over an erodible bed is formulated. We show that a crucial contribution to the lag is related to the level at which the shear stress driving bed evolution is evaluated. More precisely, following the current saltation models of bedload transport, the shear stress is evaluated at the interface between the flowing fluid and the saltation layer where grains participate in the bedload transport process. What could be considered as a minor modification of the analysis, due to the small thickness of the bedload layer, is found to alter remarkably the resulting stability plot. In particular, it turns out that antidune formation neither necessarily requires the presence of transport in suspension nor the effect of particle inertia. Some light is also shed on the debated role of gravity in the dune regime and ultimately a unified view of the process of dune and antidune formation is obtained.

The rest of the paper proceeds as follows. In § 2 and § 3 the system of equations describing the flow and the sediment transport models respectively are presented. In the latter section the level at which the Shields stress should be evaluated is also considered. In § 4 the resulting system of equations is linearized with respect to small periodic longitudinal disturbances. Results from the present theory are presented in § 5, while the last section is devoted to some concluding remarks.

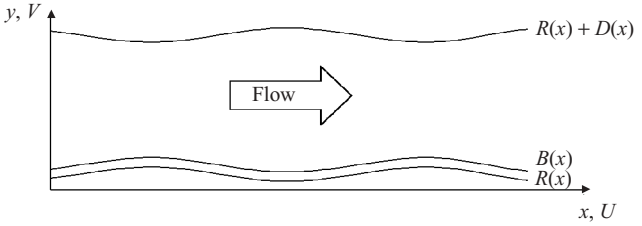

FIGURE 1. Sketch of the flow configuration.

2. Formulation of the problem: the flow model

In the framework of the well-established quasi-steady assumption, which exploits the considerable difference between the characteristic timescales of flow and bed evolution, the flow is assumed to adapt instantaneously to changes in bed elevation.

We then consider steady turbulent free-surface flow of an incompressible fluid of density ρ in a wide straight channel. Hereafter a star superscript will denote dimensional quantities. We denote by D^*, U^*, Fr, S the uniform values of flow depth, depth-averaged speed, Froude number and slope of the channel respectively. The friction velocity u_f^* and the depth-averaged velocity for the uniform flow are related to the slope and Froude number by the following law, which defines the friction coefficient C:

$$C = \frac{u_f^*}{U^*} = \frac{S^{1/2}}{Fr}. \tag{2.1}$$

The Reynolds equations in dimensionless form then are

$$UU_{,x} + VU_{,y} + P_{,x} - 1 - T_{xx,x} - T_{xy,y} = 0, \tag{2.2a}$$

$$UV_{,x} + VV_{,y} + P_{,y} + S^{-1} - T_{xy,x} - T_{yy,y} = 0, \tag{2.2b}$$

$$U_{,x} + V_{,y} = 0, \tag{2.2c}$$

where $\boldsymbol{U} = (U, V)$ is the local velocity vector averaged over the turbulence, P is the mean pressure and $\boldsymbol{T} = \{T_{ij}\}$ is the two-dimensional Reynolds stress tensor. Variables have been made dimensionless using the friction velocity u_f^*, the depth D^* of the unperturbed uniform flow and the fluid density ρ.

We refer to a Cartesian coordinate system (x, y) such as the one sketched in figure 1. The curves $y = R(x) + D(x)$ and $y = R(x)$ identify the upper and lower boundaries of the flow domain respectively, so that D represents the local flow depth. Furthermore, we stipulate that the latter boundary is set at the reference level, the level at which conventionally the mean logarithmic profile vanishes. The above system is solved with the boundary conditions of vanishing shear stress at the free surface and of vanishing velocity at the lower boundary.

The transformation of variables

$$\eta = \frac{y - R(\xi)}{D(\xi)}, \qquad \xi = x, \tag{2.3}$$

is then employed, which maps the channel sketched in figure 1 into a rectangular domain.

In order to close the above formulation we employ a Boussinesq-type assumption:

$$T_{ij} = \nu_T (U_{i,j} + V_{j,i}). \tag{2.4}$$

For the evaluation of the eddy viscosity ν_T, a formulation in terms of a mixing length is adopted:

$$\nu_T = l^2 U_{,y}, \qquad l = DL(\eta), \qquad L(\eta) = \kappa(\eta + \eta_r)(1-\eta)^{1/2}, \tag{2.5}$$

where κ is the Kármán constant.

An alternative formulation for the eddy viscosity, based implicitly on the value of the friction velocity at the reference level, has also been considered, showing a tendency to slightly overestimate the intensity of the bed shear stress perturbation. The mixing-length approach (2.5) has thus been chosen to produce the results presented herein.

In (2.5), the quantity η_r, which sets the value of the mixing length at the reference level, is the non-dimensional distance between the reference level and the local value of the mean bed elevation and is related to bed roughness.

Restricting our attention to the simple case of a uniform flow over a flat bed composed of well-packed spheres of non-dimensional diameter d_s, sketched in figure 2(a), the law of the wall can be written as

$$U = \frac{1}{\kappa} \ln\left(\frac{y}{k_s}\right) + K = \frac{1}{\kappa} \ln\left(\frac{y}{y_r}\right), \tag{2.6}$$

where k_s is the the non-dimensional roughness height.

The quantity y_r can thus be estimated, by simple comparison, as a function of the constant K. The universally accepted value of 8.5 for K leads to a value of y_r that is about one thirtieth of the roughness height, which in turn can be estimated as 2.5 times the grain size, leading to $y_r = d_s/12$.

Moreover, the origin of the vertical axis is set at the average bed level, which is at a distance of $d_s/6$ below the top of the grains. Hence, the reference level is inside the roughness elements, and the logarithmic profile expressed by (2.6) cannot be thought as representative of the real velocity profile in a region which is of the order of the sediment diameter.

3. Formulation of the problem: the sediment transport model

As far as bed dynamics is concerned, only bedload transport is considered herein and a new formulation is introduced that deserves some introductory arguments.

In the work of Bagnold (1956), which can be considered as the first mechanistic approach to sediment transport, "the rate of work done in pushing the bedload along the bed against frictional resistance" was related to "the power in the flow available to move the sediment", leading to a relationship between the sediment discharge per unit width and the bed shear stress. Bagnold's idea can be easily explained in term of a conceptual experiment like the one presented in figure 2.

Suppose we have a uniform flow above a fixed bed of homogeneous roughness as sketched in figure 2(a), where the behaviour of the shear stress in the neighbourhood of the bed is also shown. Note that the shear stress reaches its maximum τ_r at the reference level R, which is situated slightly below the top of the grains. As already mentioned, this situation is not physically representative in the neighbourhood of the grains but simply fits the value of the constant K for the logarithmic profile of velocity expressed by (2.6).

In Bagnold's ideal experiment, as shown in figure 2(b), we now allow the bed to suddenly become cohesionless, feeding, into the same time, sediments into the upstream section. Moreover, we stipulate that sediments are fed at a rate that exactly

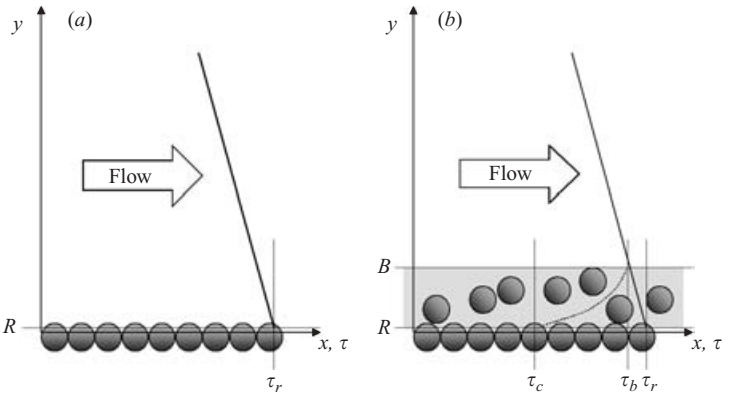

FIGURE 2. Sketch of the sediment transport model: (*a*) a fixed bed; (*b*) a cohesionless bed.

balances the flow capacity to transport sediments, whatever this capacity might be. If only bedload transport is allowed, as assumed herein, we know that sediments move by small jumps (saltation) confined in a region close to the bed defined as the 'bedload' or 'saltation' layer. Since the average bedload discharge is uniform, again the average bed surface experiences neither aggradation nor degradation or, more precisely, erosion and deposition rates statistically balance each other. Above this bedload layer we have clear fluid in uniform motion, such that the shear stress distribution is identical to that depicted in figure 2(*a*). We define the top of the bedload layer as B and the shear stress at this level as τ_b.

Inside the bedload layer, the shear stress drops, this reduction being representative, from an energy point of view, of the power spent by the flow in moving the sediments. Whether such a reduction leads the external stress τ_b to decrease down to the critical value τ_c, as Bagnold suggested, or to a somewhat higher value as recently pointed out (Seminara, Solari & Parker 2002) is irrelevant in the present context.

According to the above ideas, the shear stress exerted by the fluid on the sediments moving in the bedload layer should be evaluated at level B. In other words, it is the stress τ_b and not the stress τ_r which should be used to estimate the bedload discharge. Due to the small thickness of the bedload layer, the difference in modulus between τ_b and τ_r is typically so small that it can safely be neglected. Nonetheless, it will appear that the phase of the shear stress relative to bed elevation, which drives the instability process, varies significantly in the neighbourhood of the reference level, so that this assumption can lead to incorrect predictions when the vertical structure of the flow, as in the case of dunes, is used for the determination of the transporting shear stress.

A new parameter is then introduced in the analysis, namely the thickness of the bedload layer under uniform flow conditions h_b, which can be safely set to be proportional to the non-dimensional grain size d_s:

$$h_b = l_b d_s. \tag{3.1}$$

Hence, h_b identifies the position of the interface that separates the upper clear-water layer from the lower bedload layer, in which the two-phase (sediment and water) flow is confined. In the above two-layer formulation it is implicitely assumed that the clear-water flow is unaffected by the presence of the bedload layer and that the sediment discharge that takes place in the latter is uniquely determined by the shear stress exerted by the fluid on the interface and by the sediment characteristics. This formulation, which constitutes the basis for most of the movable-bed models available

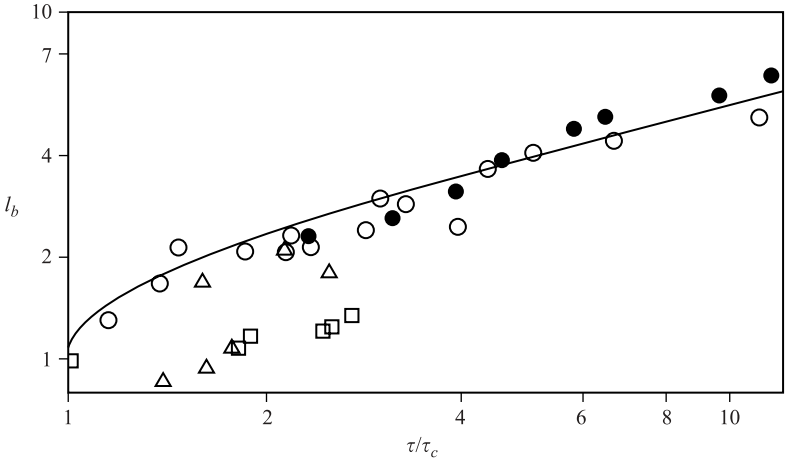

FIGURE 3. Dimensionless maximum saltating height versus τ/τ_c. Experiments: ○, Sekine & Kikkawa (1992); ●, Lee & Hsu (1994); △, Niño, Garcia & Ayala (1994); □, Niño & Garcia (1998); solid line is (3.2) with $A_b = 1.3$ and $m = 0.55$.

in the literature, establishes the simplest possible link between flow and bed dynamics: a modification of bed elevation drives a modification of the fluid flow, which produces a change in the shear stress at the interface and then in the local transport capacity, which in turn modifies bed elevation. A more detailed analysis of the two-phase flow that takes place close to the bed and of the saltating grain dynamics will undoubtely provide a more refined description of the complex sediment–water interactions that ultimately drive bed evolution. Although crude, however, the two-layer formulation adopted herein seems able to grasp at least the main features of the mechanism of bedform formation.

In figure 3, some experimental observations of l_b are shown as a function of the ratio of the bed shear stress and its critical value. It can be seen that the experimental points show a consistent trend, even though some scatter is present, expecially for low values of the bed shear stress, i.e. close to the threshold of motion. It must be noted that there is some uncertainty in the definition of the saltation height in the various experiments. In fact, as Sekine & Kikkawa (1992) pointed out, the "averaged saltation height" can be defined either as "the ensemble average of the maximum saltation height over an entire step length", providing experimental measurements of the thickness of the saltating bedload layer h_b, or as "the averaged elevation above the bed of a saltating grain", the latter being clearly lower than the former.

On the basis of the experimental observations, it turns out that l_b is an increasing function of the bed shear stress, which can be written in the form

$$l_b = 1 + A_b \left(\frac{\tau_r - \tau_c}{\tau_c} \right)^m, \qquad \tau_r \geqslant \tau_c. \tag{3.2}$$

In the following, the value of the constant A_b and of the exponent m have been set equal to 1.3 and to 0.55 respectively, on the basis of a regression analysis on the experimental data of Sekine & Kikkawa (1992) and of Lee & Hsu (1994), which are shown as open and solid circles in figure 3, respectively. The above evaluation of the exponent m is confirmed by Lee & Hsu (1994), who proposed a relationship analogous to (3.2) with a value of m equal to 0.575 and by the simulations of Lee,

You & Lin (2002), who proposed the value of 0.511 on the basis of a regression analysis on computer simulated data.

The experiments of Niño & Garcia (1998) and of Niño, Garcia & Ayala (1994) exhibit a much weaker dependence of the saltating height on the ratio τ_b/τ_c. Apart from the above-mentioned uncertain definition of the measured quantity, this may also be due to the role of the particle Reynolds number, which has been neglected in (3.2).

Under the above assumptions, the Exner equation of sediment mass conservation, can be written as

$$B_{,t} = -\Phi_{,x}, \tag{3.3}$$

where Φ is the dimensionless sediment discharge per unit width,

$$\Phi = \frac{q_s^*}{d_s^*\sqrt{(s-1)gd_s^*}}, \tag{3.4}$$

and time has been made non-dimensional using the sediment characteristic slow timescale

$$\widehat{t} = \frac{D^{*2}(1-\lambda_p)}{d_s^*\sqrt{(s-1)gd_s^*}}. \tag{3.5}$$

In the above equations, g is gravitational acceleration while d_s^*, s and λ_p are diameter, relative density and porosity of the sediment, respectively.

In order to close the problem, a suitable relationship between the sediment discharge Φ and the flow must be introduced. Several formulations for the function Φ are available in the literature, all exhibiting a dependence by some power on a dimensionless form of the shear stress acting on the bed, known as the Shields stress θ_b:

$$\theta_b = \frac{\tau_b^*}{\rho(s-1)gd_s^*}. \tag{3.6}$$

Results of the linear stability theory are only moderately affected by the choice of a particular form of the function Φ. In the following, the Meyer-Peter & Müller formula

$$\Phi = 8(\theta_b - \theta_c)^{3/2} \tag{3.7}$$

has been employed, where θ_c is the critical Shields stress for incipient motion.

Finally, when only bedload transport is considered, as in the present case, gravity favours the downhill motion of the grains and conversely opposes the uphill motion. Following Fredsøe (1974), this effect has been accounted for by modifying the critical Shields stress θ_c in the form

$$\theta_c = \theta_{ch} - \mu(S - B_{,x}), \qquad \mu = \frac{\theta_{ch}}{\tan\Psi}, \tag{3.8}$$

where θ_{ch} has been set equal to the conventional value for a horizontal bed (0.047) and Ψ is the friction angle. An appropriate estimate for μ is about 0.1 (Fredsøe 1974).

4. Linearization

We now assume the following normal-mode representation for the generic perturbed property F:

$$F(\xi, \eta, t) = F_0(\eta) + \epsilon F_1(\xi, \eta, t), \tag{4.1a}$$

$$F_1(\xi, \eta, t) = f(\eta)\exp[\mathrm{i}(\alpha\xi - \Omega t)] + \text{c.c.} \tag{4.1b}$$

with the parameter ϵ chosen to be small in accordance with the assumption of small perturbations of the uniform configuration. In the above, α is the wavenumber of the perturbation, Ω the complex growth rate and c.c. stands for the complex conjugate of the preceding quantity.

The above expansion can then be substituted into the governing equations, boundary conditions and closure assumptions to obtain a sequence of problems at the various orders of approximation in the small parameter ϵ. We skip the details of this procedure, which is tedious but standard, and simply show the main results.

4.1. $O(\epsilon^0)$

At leading order the system of differential equations and boundary conditions for the basic uniform flow can be rewritten as

$$T'_{t0} = -1, \qquad T'_{n0} = -S^{-1}, \tag{4.2}$$

$$U_0|_{\eta=0} = 0, \qquad T_{t0}|_{\eta=1} = 0, \qquad T_{n0}|_{\eta=1} = 0, \tag{4.3}$$

where

$$T_{t0} = \nu_{T0} U'_0, \qquad T_{n0} = -P_0 \tag{4.4}$$

are the stresses tangential and normal to surfaces at constant η respectively and primes denote differentiation with respect to η.

Linearization of the eddy viscosity relationship (2.5) leads to

$$\nu_{T0} = l_0^2 U'_0, \qquad l_0 = L = \kappa(\eta + \eta_r)(1-\eta)^{1/2}. \tag{4.5}$$

The above system immediately integrates to yield

$$U_0 = \frac{1}{\kappa} \ln\left(\frac{\eta + \eta_r}{\eta_r}\right), \qquad P_0 = S^{-1}(1-\eta), \tag{4.6}$$

i.e. the classic rough logarithmic law for the velocity and the hydrostatic distribution for pressure.

By comparison with (2.6) we easily find that the quantity η_r is identical to y_r so that

$$R_0 = \eta_r = \frac{k_s}{30} = \frac{d_s}{12}. \tag{4.7}$$

Integrating the vertical profile of velocity once more, we obtain

$$\overline{U_0} = \frac{U^*}{u_f^*} = \frac{1}{C} = \frac{1}{\kappa}\left[\ln\left(\frac{1+\eta_r}{\eta_r}\right) - 1\right], \tag{4.8}$$

which relates the friction coefficient C to η_r.

Exner's equation (3.3) does not produce any additional information at the leading order since under uniform flow conditions the bed experiences neither aggradation nor degradation. It is worth mentioning that

$$\eta_b = B_0 - R_0 = \frac{d_s}{12} + h_b, \tag{4.9}$$

where h_b is the thickness of the bedload layer introduced in § 3. The quantity η_b thus represents the non-dimensional distance between level B and level R. Moreover, the following relationships hold:

$$\theta_{b0} = \theta_{r0}(1-\eta_b), \qquad \theta_{r0} = \frac{C^2 Fr^2}{(s-1)d_s} = \frac{S}{(s-1)d_s}, \tag{4.10}$$

so that enforcing $\eta_b = 0$ corresponds to evaluate the bed shear stress at the reference level R.

4.2. $O(\epsilon^1)$

It is convenient to introduce the new variables

$$T_t = \nu_{T0}\left(u' - U_0' d + \mathrm{i}\alpha v + \frac{\nu_T}{\nu_{T0}} U_0'\right), \qquad T_n = -p - 2\mathrm{i}\alpha\nu_{T0} u, \tag{4.11}$$

which represent the amplitudes of the perturbed stresses tangential and normal to surfaces at constant η, respectively. In the above u, v are the longitudinal and vertical components of the perturbed velocity, while p and d are the amplitudes of the pressure and flow depth perturbation. Finally, the ratio ν_T/ν_{T0} follows from the perturbation of (2.5):

$$\frac{\nu_T}{\nu_{T0}} = \frac{u'}{U_0'} + d. \tag{4.12}$$

After some manipulations, a system of ordinary differential equations is eventually obtained that can be written in the general form

$$\mathscr{L}\boldsymbol{Z} = d\boldsymbol{D} + r\boldsymbol{R}, \tag{4.13}$$

where d is considered as a parameter to be determined and r represents the amplitude of the perturbation of the reference level. The vector $\boldsymbol{Z}$ of the unknowns is

$$\boldsymbol{Z} = (u, v, T_t, T_n)^T. \tag{4.14}$$

The linear differential operator $\mathscr{L}$ in (4.13) is

$$\mathscr{L} = \begin{pmatrix} \mathrm{d}/\mathrm{d}\eta & \mathrm{i}\alpha/2 & -1/(2\nu_{T0}) & 0 \\ \mathrm{i}\alpha & \mathrm{d}/\mathrm{d}\eta & 0 & 0 \\ -\mathrm{i}\alpha U_0 - 4\alpha^2\nu_{T0} & -U_0' & \mathrm{d}/\mathrm{d}\eta & \mathrm{i}\alpha \\ 0 & -\mathrm{i}\alpha U_0 & \mathrm{i}\alpha & \mathrm{d}/\mathrm{d}\eta \end{pmatrix}, \tag{4.15}$$

while the vectors $\boldsymbol{D}$ and $\boldsymbol{R}$ are, respectively,

$$\boldsymbol{D} = \begin{pmatrix} 0 \\ \mathrm{i}\alpha U_0'\eta \\ (-\mathrm{i}\alpha U_0 U_0' + \mathrm{i}\alpha S^{-1} - 2\alpha^2(1-\eta))\eta - 1 \\ S^{-1} + \mathrm{i}\alpha\eta - 2\mathrm{i}\alpha(1-\eta) \end{pmatrix} \tag{4.16}$$

and

$$\boldsymbol{R} = \begin{pmatrix} 0 \\ \mathrm{i}\alpha U_0' \\ -\mathrm{i}\alpha U_0 U_0' + \mathrm{i}\alpha S^{-1} - 2\alpha^2(1-\eta) \\ \mathrm{i}\alpha \end{pmatrix} \tag{4.17}$$

Linearization of the boundary conditions yields the vanishing of u and v at the reference level ($\eta = 0$), while at the free surface ($\eta = 1$) we have

$$v = \mathrm{i}\alpha U_0(r + d), \qquad T_t = 0, \qquad T_n = 0. \tag{4.18}$$

Linearity of the differential system allows us to express its solution in the form

$$\boldsymbol{Z} = c_1\boldsymbol{Z}_1 + c_2\boldsymbol{Z}_2 + d\boldsymbol{Z}_\mathrm{d} + r\boldsymbol{Z}_\mathrm{r}. \tag{4.19}$$

Thus $\boldsymbol{Z}$ is a linear combination of two linearly independent solutions of the homogeneous initial value problem

$$\mathscr{L}\boldsymbol{Z}_{1,2} = 0, \tag{4.20}$$

each satisfying the boundary conditions at the lower boundary, plus particular solutions of the non-homogeneous differential systems

$$\mathscr{L}\boldsymbol{Z}_d = \boldsymbol{D}, \qquad \mathscr{L}\boldsymbol{Z}_r = \boldsymbol{R}, \tag{4.21}$$

again satisfying the lower boundary conditions.

Using the splitting (4.19) on the boundary conditions at the free surface (4.18), a linear 3×3 non-homogeneous algebraic system in the three unknowns c_1, c_2 and d is found, the solution of which is proportional to r. We then readily obtain

$$(c_1, c_2, d, r)^T = r(T_{tr}, T_{nr}, D, 1)^T = r\boldsymbol{X}, \tag{4.22}$$

where the two linearly independent solutions of the homogeneous problem (4.20) have been chosen so that the unknowns c_1 and c_2 are the values of the perturbation of the tangential and normal stress at the reference level, respectively. The vector $\boldsymbol{X}$ thus provides the 'forced' response of the flow to a unit reference level perturbation.

Linearization of the sediment continuity equation yields the following equation:

$$\Omega b = \alpha\phi, \tag{4.23}$$

where b is the amplitude of the perturbation of the active layer thickness, which is identical to r since B and R are both proportional to the uniform sediment grain diameter and thus kept at a constant distance from one another, 'moving' together as the bed evolves.

The amplitude ϕ of the perturbation of the bedload discharge Φ defined by (3.7) can be expanded as in (4.19), leading to

$$\phi = (\phi_1 c_1 + \phi_2 c_2 + \phi_d d + \phi_r r) = \boldsymbol{\phi} \cdot (c_1, c_2, d, r)^T = \boldsymbol{\phi} \cdot \boldsymbol{X} r, \tag{4.24}$$

where

$$\phi_1 = \left[\frac{\partial \Phi}{\partial c_1}\right]_0 = \left[\frac{\partial \Phi}{\partial \theta_b}\frac{\partial \theta_b}{\partial c_1} + \frac{\partial \Phi}{\partial \theta_c}\frac{\partial \theta_c}{\partial c_1}\right]_0 = \left[\frac{\partial \Phi}{\partial \theta_b}\right]_0 \left[\frac{\partial (\theta_b - \theta_c)}{\partial c_1}\right]_0 \tag{4.25}$$

and the suffix 0 stands for 'evaluated at base condition'. Analogous relationships hold for ϕ_2, ϕ_d and ϕ_r.

Expanding also the perturbed shear stress T_{tb} as in (4.19) we then readily obtain

$$\boldsymbol{\phi} = A\left(T_{tb1}, T_{tb2}, T_{tbd} + \eta_b, T_{tbr} - \mathrm{i}\alpha\frac{\mu}{\theta_{r0}}\right)^T, \tag{4.26}$$

where T_{tb1}, T_{tb2}, T_{tbd} and T_{tbr} are evaluated at η_b and

$$A = \left[\frac{\partial \Phi}{\partial \theta_b}\right]_0 \theta_{r0}, \tag{4.27}$$

Making use of (4.24) and (4.26), we can rewrite (4.23), obtaining the dispersion relationship

$$\Omega = \alpha\boldsymbol{\phi} \cdot \boldsymbol{X}, \tag{4.28}$$

and solving for the imaginary part of the growth rate we finally obtain

$$\Omega^i = \alpha^2 A\left(\frac{T_{tb}^i + \eta_b D^i}{\alpha} - \frac{\mu}{\theta_{r0}}\right), \tag{4.29}$$

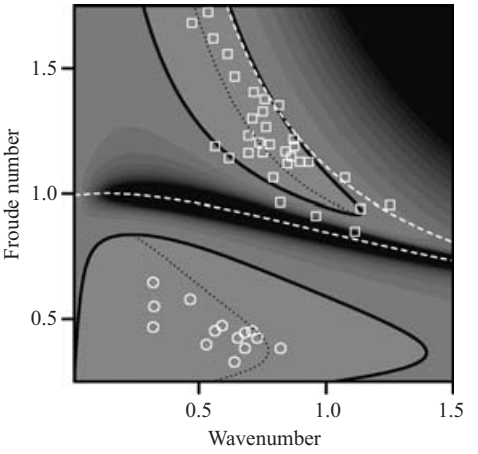

FIGURE 4. Growth rate plot: comparison of the results of the present theory with the experiments of Guy *et al.* (1966): ○, dunes; □, antidunes.

which clearly shows how instability is related to a balance between destabilizing and stabilizing effects. In fact, the first term on the right-hand side of (4.29) is associated with the action of the tangential bed shear stress so that instability is found when it lags behind dune crests (i.e. when its imaginary part is positive); on the contrary, the second term, which is associated with the action of gravity, always acts to reduce instability. The reader will note that, on letting η_b vanish, T_{tb} becomes equal to T_{tr} and the formulation of classic linear theories (Fredsøe 1974; Richards 1980) is recovered.

5. Discussion of the results

We now move to the results obtained in the framework of the linear theory described in the previous section. Figure 4 shows a comparison of the result of the present model with the experiments of Guy, Simons & Richardson (1966) as reported by Fredsøe (1974). The parameters of the simulation are the same as in the analysis presented in the latter paper (i.e. $C^{-1} = 20$, $\mu = 0.1$). Growth rate is shown in shades of grey, lighter colours corresponding to higher values.

Two regions of instability appear, which are bounded by the marginal curves (vanishing growth rate) represented as thick solid lines in the plot. The broken white lines are the curves of vanishing celerity and delimit three regions in the plot: below the lower curve and above the upper curve, wave celerity is positive (downstream migration) while it is negative (upstream migration) in the region bounded by the two curves. Moreover, all the unstable disturbances lying above the lower broken line are characterized by a phase-lag between the free surface and the bed elevation of less than $\pi/2$ in modulus (antidunes) while the opposite is true for disturbances lying below the line (dunes).

The agreement with the experimental data is fairly good: almost the whole set of measurements, for both dune and antidunes, falls inside the appropriate region of instability, grouping along the lines of maximum amplification (dotted lines). Dunes are found to always migrate downstream while antidunes migrate mostly upstream, even though the upper curve of vanishing celerity crosses the marginal curve for antidune instability, hence allowing downstream migrating antidunes at larger Froude numbers.

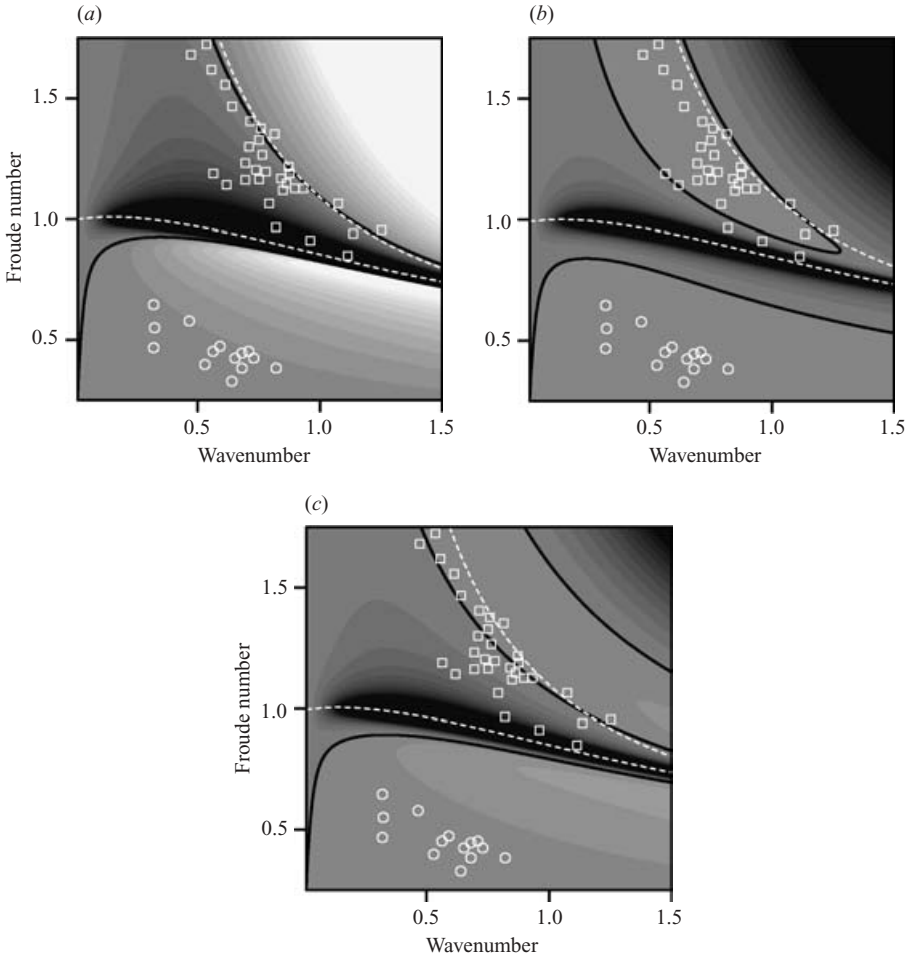

FIGURE 5. Growth rate in the (Fr, α)-space: (*a*) $\Omega^i = A\alpha^2(T)$, $\eta_b = 0$; (*b*) $\Omega^i = A\alpha^2(T+P)$, $\eta_b = d_s/12 + h_b$; (*c*) $\Omega^i = A\alpha^2(T+P)$, $\eta_b = d_s/12 + h_b/2$. Experiments of Guy *et al.* (1966): ○, dunes; □, antidunes.

It is interesting at this point to investigate in more detail the effects of the key assumption presented in § 3 concerning the level at which the bed shear stress must be evaluated. In order to make this dependence explicit, it is useful to rewrite (4.29) as follows:

$$\Omega^i = \alpha^2 A(T + P - G), \tag{5.1}$$

where

$$T = \frac{T^i_{tr}}{\alpha}, \qquad P = \frac{T^i_{tb} + \eta_b D^i - T^i_{tr}}{\alpha}, \qquad G = \frac{\mu}{\theta_{r0}}. \tag{5.2}$$

If only the term T is considered in the analysis (i.e. if the bed shear stress is evaluated at the reference level and the effect of gravity is neglected) the growth rate plot shown in figure 5(*a*) is obtained. The values of the parameters are the same as in figure 4.

Note that, when a rotational flow model is adopted, we are faced with a somewhat reversed problem with respect to the potential-flow formulation: the destabilizing term

associated with the phase-lag of the bed shear stress is so intense that it becomes difficult to stabilize it in the short-wavelength range, a necessary condition to obtain realistic predictions for dune and antidune wavelengths.

In the dune regime, Fredsøe (1974) provided a realistic comparison with experimental data on dune wavelength. In that case, the effect of gravity was included in the formulation on the basis of available treatments of the effect of bedslope on bedload transport (i.e. using (3.8)), but the flow model employed was based on a slip velocity approach, known to sharply underestimate the bed shear stress. When a more refined flow model was adopted (Richards 1980), the intensity of the stabilizing effect associated with gravity had to be at least an order of magnitude larger than that assumed by Fredsøe (1974), an unjustified and unrealistic assumption.

In the antidune regime, all previous theories agree on the fact that gravity should play a minor role, so that other stabilizing effects have been invoked such as the presence of suspended load (Engelund & Fredsøe 1974). In this regard, we should point out that antidunes are easily observed both in nature and in the laboratory in the absence of suspended load. Particle inertia provides, in this regime, a further destabilizing effect, so that its inclusion does not lead to any damping.

If the new term P, which accounts for evaluating the bed shear stress on the top of the active layer, is included in the analysis, the growth rate plot changes remarkably as shown in figure 5(b). A comparison with figure 5(a) shows that the instability regions for both dunes and antidunes are now much more consistent with the experimental observations. Note that the only difference between the two formulations lies in the assumption of a finite (though small) rather than negligible thickness of the bedload layer. In order to estimate the sensitivity of the model to the bedload layer thickness h_b, its value has been arbitrarily halved, producing the plot presented in figure 5(c). While an overall damping in the short-wavelength range is clearly detectable also in this plot, the agreement with the experimental observations is poorer. This indirectly confirms that the evaluation of h_b through (3.1) and (3.2) provides the best description of the sediment transport dynamics, at least in the formulation adopted in the present work.

Figure 6 shows the behaviour of the real and imaginary parts of the perturbation of the tangential shear stress in a neighbourhood of the reference level for several values of the Froude number. The vertical coordinate is scaled with the thickness of the bedload layer and the value of the wavenumber is set equal to 1. Inside the bedload layer the real part of the perturbation, which is associated with the celerity of the sand wave, is only slightly modified. On the contrary, the imaginary part, which is associated with the growth or decay of the perturbation, changes remarkably, so that disturbances that are stable at the reference level become unstable at the top of the saltation layer and vice versa. Note that the latter variation is particularly strong in the dune regime, where the bedload layer is just a few grain diameters thick.

It should be pointed out that the shaded areas in the plots represent the region occupied by the bedload layer, but the flow solution shown is relative to the case of clear-water flow. Under the assumption that the flow above the layer is unaffected by the presence of the layer itself, which is implicit in the two-layer formulation adopted, this allows the determination of the phase-lag that ultimately drives bed evolution.

Expanding in Taylor series the imaginary part of the perturbed tangential stress T_t in a neighbourhood of the reference level we readily obtain

$$\alpha P = T^i_{tb} + \eta_b D^i - T^i_{tr} = \left(T^i_{tr,\eta} + D^i\right)\eta_b = -\alpha\left(T^r_{nr} - S^{-1}\right)\eta_b = P^i_{r,x}\eta_b, \tag{5.3}$$

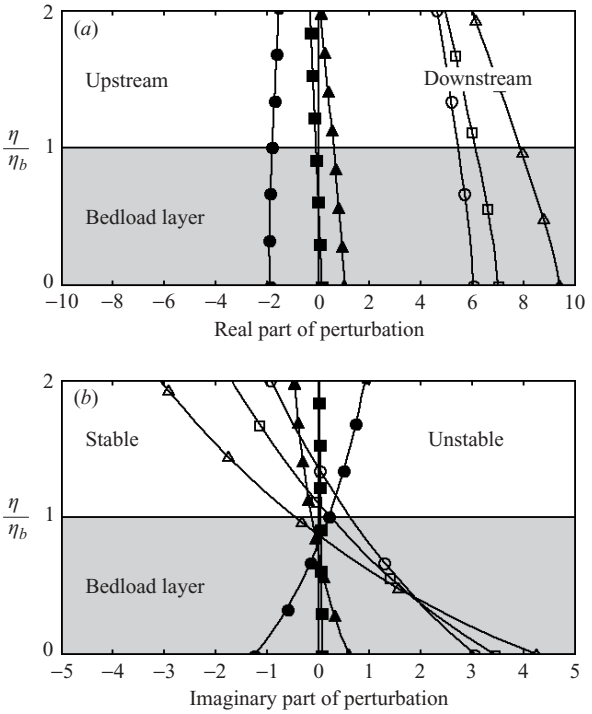

FIGURE 6. (*a*) Real and (*b*) imaginary parts of the amplitude of the shear stress perturbation as a function of vertical distance in the neighbourhood of the reference level; $\alpha = 1$: ○, $Fr = 0.5$; □, $Fr = 0.6$; △, $Fr = 0.7$; ●, $Fr = 1$; ■, $Fr = 1.1$; ▲, $Fr = 1.2$.

where $P_{r,x}$ represents the perturbation of the longitudinal pressure gradient evaluated at the reference level. The physical mechanism which leads to the appearance of the term P is then found in terms of a simple force balance for a fluid particle located close to the reference level: the longitudinal pressure gradient generated by the perturbation in bed elevation acts to modify the tangential shear stress when moving away from the bed.

Finally, if the effect of gravity is also included in the analysis, the growth rate plot shown in figure 4 is obtained ($\mu = 0.1$). A direct comparison with the analogous figure 5(*b*), where the effect of gravity was neglected, shows that gravity is relevant only for small values of the Froude number ($Fr \leqslant 0.4$). It may be worth noting that gravity should indeed play a minor role in the antidune regime as already pointed out by Fredsøe (1974).

6. Conclusions

The present revisiting of the linear theory of sand dunes has clarified a few of the obscure aspects of classical approaches, representing a step forward in the understanding of the instability process that drives dune and antidune formation.

Firstly, if the bed shear stress is evaluated at the top of the bedload layer, a new term, which is related to the role of the longitudinal pressure gradient, formally enters the analysis. This choice is consistent with Bagnold's approach to sediment transport. The real part of the perturbation of the bed shear stress is almost unaffected by this procedure while its imaginary part, which only contributes to instability, changes

rapidly in the neighbourhood of the reference level so that the delicate balance between destabilizing and stabilizing effects is crucially affected by this choice. This result seems to us to be of some relevance and suggests that movable-bed models based on three-dimensional flow solutions should account for the new hypothesis proposed in the present paper.

Secondly, the formation of antidunes requires neither the presence of suspended load nor the effect of sediment inertia, though both these effects may alter the stability plot. Dunes and antidunes are shown to form in the same conceptual framework and the wavelengths of maximum amplification predicted by the theory are in good agreement with the experimental measurements in both regimes.

Thirdly, the stabilizing effect of gravity on bedload transport turns out to be much less important than in previous linear theories provided that perturbations of sediment transport are based on the above procedure.

In a recent contribution, Coleman & Fenton (2000) have shown that coupling flow and bed evolution leads to another source of lag between sediment transport and bed topography. Indeed, the quasi-steady flow assumption that justifies the decoupling procedure completely rules out any mode of instability associated with the flow, possibly leading to incomplete predictions. In fact, an unrealistic resonant behaviour, which appears as a deep valley (the darkest area in figure 4, for example) in the growth rate surface plots, is found in the neighbourhood of the line describing steady flow perturbations (which is essentially coincident with the lower white dashed line in the same figure). Preliminary calculations obtained by means of the present model retaining time derivatives in the flow equations have shown that, even though the unrealistic resonance disappears in the coupled solution, the shape of the unstable regions in the parameter space is only moderately affected by the coupling. More precisely, as in Coleman & Fenton (2000), changes are confined within a thin region surrounding the line of steady flow perturbation. Howevver, in contrast with the results of the above potential flow analysis, stability of the uniform flow is found by the present rotational theory in the latter region.

Needless to say, a linear theory is unable to clarify further features related to dune development, most importantly its ability to reach an equilibrium amplitude. In this respect, a feature which will require attention is the role of flow separation in the selection of dune wavelength. Whether this is able to prevail over the linear mechanism of selection of normal-mode perturbations is a question which remains open, even though the good agreement between the results of the present linear theory and the experimentally observed wavelengths of finite-amplitude dunes and antidunes is encouraging in this regard.

The author wishes to thank Professor G. Seminara and Professor M. Tubino for interesting discussions in connection with the problem of dune instability. This research was partially supported by the Italian Ministero dell'Istruzione, dell'Università e della Ricerca (Project COFIN 2001) and by the Fondazione Cassa di Risparmio di Verona, Vicenza, Belluno ed Ancona (Project RIMOF).

REFERENCES

Bagnold, R. A. 1956 The flow of cohesionless grains in fluids *Phil. Trans. R. Soc. Lond.* A **249**, 235–297.

Blondeaux, P. & Seminara, G. 1985 A unified bar-bend theory of river meanders. *J. Fluid Mech.* **157**, 449–470.

Callander, R. A. 1969 Instability and river channels. *J. Fluid Mech.* **36**, 465–480.

Coleman, S. E. & Fenton, J. D. 2000 Potential-flow instability theory and alluvial stream bed forms. *J. Fluid Mech.* **418**, 101–117.

Colombini, M. 1993 Turbulence-driven secondary flows and formation of sand ridges. *J. Fluid Mech.* **254**, 701–719.

Colombini, M. & Parker, G. 1995 Longitudinal streaks. *J. Fluid Mech.* **304**, 161–183.

Engelund, F. 1970 Instability of erodible beds. *J. Fluid Mech.* **42**, 225–244.

Engelund, F. & Fredsøe, J. 1974 Transition from dunes to plane bed in alluvial channels. *Tech. Univ. Denmark, Inst. Hydrodyn. and Hydraulic Engng, Series paper* 4.

Engelund, F. & Fredsøe, J. 1982 Sediment ripples and dunes *Annu. Rev. Fluid Mech.* **14**, 13–37.

Fredsøe, J. 1974 On the development of dunes in erodible channels. *J. Fluid Mech.* **64**, 1–16.

Gradowczyk, M. H. 1970 Wave propagation and boundary instability in erodible-bed channels. *J. Fluid Mech.* **33**, 93–112.

Guy, H. P., Simons, D. B. & Richardson, E. V. 1966 Summary of alluvial channel data from flume experiments 1956–61. *Geol. Survay Prof. Paper* 462-I, pp. 1–96.

Hayashi, T. 1970 Formation of dunes and antidunes in open channels. *J. Hydraul. Div. ASCE* **96**, 357–366.

Ikeda, S., Parker, G. & Sawai, K. 1981 Bend theory of river meanders. Part 1. Linear development. *J. Fluid Mech.* **112**, 363–377.

Kennedy, J. F. 1963 The mechanism of dunes and antidunes in erodible-bed channels. *J. Fluid Mech.* **16**, 521–544.

Kennedy, J. F. 1969 The formation of sediment ripples, dunes and antidunes. *Annu. Rev. Fluid Mech.* **1**, 147–168.

Lee, H.-Y. & Hsu, I.-S. 1994 Investigation of saltating particle motion. *J. Hydraulic Engng* **120**, 831–845.

Lee, H.-Y., You, J.-Y. & Lin, Y.-T. 2002 Continuous saltating process of multiple sediment particles. *J. Hydraulic Engng* **128**, 443–450.

Niño, Y. & Garcia, M. 1998 Experiments on saltation of sand in water. *J. Hydraulic Engng* **124**, 1014–1025.

Niño, Y., Garcia, M. & Ayala, L. 1994 Gravel saltation 1. Experiments. *Water Resour. Res.* **30**, 1907–1914.

Parker, G. 1975 Sediment inertia as cause of river antidunes. *J. Hydraul. Div. ASCE* **101**, 211–221.

Richards, K. J. 1980 The formation of ripples and dunes on an erodible bed. *J. Fluid Mech.* **99**, 597–618.

Sekine, M. & Kikkawa, H. 1992 Mechanics of saltating grains. *J. Hydraulic Engng* **118**, 536–558.

Seminara, G., Colombini, M. & Parker, G. 1996 Nearly pure sorting waves and formation of bedload sheets. *J. Fluid Mech.* **312**, 253–278.

Seminara, G., Solari, L. & Parker, G. 2002 Bedload at low Shields stress on abitrarily sloping beds:failure of the Bagnold hypothesis. *Water Resour. Res.* **38**, art. 1249.

Smith, J. D. 1970 Stability of a sand bed subjected to a shear flow at low Froude number. *J. Geophys. Res.* **75**, 5928–5940.

Sumer, B. M. & Bakioglu, M. 1984 On the formation of ripples on an erodible bed. *J. Fluid Mech.* **144**, 177–190.

Tsujmoto, T. 1989 Longitudinal stripes of sorting due to cellular secondary currents. *J. Hydrosci. Hydraul. Engng* **7**, 1, 23–34.